PCCP

Surface plasmon resonance of silver and gold nanoparticles in proximity of graphene studied with the discrete dipole approximation method

SCHOLARONE™
Manuscripts

Surface plasmon resonance of silver and gold nanoparticles in proximity of graphene studied with the discrete dipole approximation method

Vincenzo Amendola*

Department of Chemical Sciences, Università di Padova, via Marzolo 1, I-35131 Padova, Italy

* correspondence: vincenzo.amendola@unipd.it

Abstract.

The integration of silver and gold nanoparticles with graphene is frequently sought for the realization of hybrid materials with superior optical, photoelectric and photocatalytic performances. A crucial aspect for these applications is how the surface plasmon resonance of metal nanoparticles is modified after assembly with graphene. Here, we used the discrete dipole approximation method to study the surface plasmon resonance of silver and gold nanoparticles in proximity of a graphene flake or embedded in graphene structures. Surface plasmon resonance modifications were investigated for various shapes of metal nanoparticles and for different morphologies of the nanoparticle-graphene nanohybrids, in a step-by-step approach. Calculations show that surface plasmon resonance of Ag nanoparticles is quenched in nanohybrids, whereas either surface plasmon quenching or enhancement can be obtained with Au nanoparticles, depending on the configuration adopted. However, graphene effects on the surface plasmon resonance are rapidly lost already at a distance of the order of 5 nm. These results provide useful indications for characterization and monitoring the synthesis of hybrid nanostructures, as well as for the development of hybrid metal nanoparticles / graphene nanomaterials with desired optical properties.

1

Introduction.

Silver and gold nanoparticles (NPs) occupy a prominent role in nanotechnology due to their favourable combination of physical-chemical properties,[1-3] such as high electric and thermal conductivity, simple surface chemistry, thermal and chemical stability and the wide gamut of effects deriving from the excitation of the surface plasmon resonance (SPR) by visible light, i.e. large extinction cross section, local electromagnetic field amplification and hot-electrons injection in nearby nanomaterials.[1-4]

Graphene shares some features with plasmonic metal NPs, such as the high physical-chemical stability and the appreciable electric and thermal conductivity.[5] In addition, graphene possess mechanical properties superior to other organic materials, constant absorption in the visible-NIR range with negligible reflectance, large surface area and electronic structure suitable for integration with other nanomaterials in electric or photoelectric devices.[6-10]

In recent years, many efforts have been directed to the combination of silver and gold NPs with graphene at different levels of structural complexity.[5, 11] The main approaches to obtain nanohybrids are graphene transfer on a pre-deposited metal NPs array,[12-18] *in situ* growth of metal nanostructures directly on graphene,[5, 19-22] or mixing of already formed metal NPs with graphene, often after proper surface functionalization.[5, 23] By similar approaches, hybrid plasmonic nanostructures are achieved also with graphene derivatives such as graphene oxide.[24, 25]

These composite nanomaterials showed new optical properties, ranging from the amplification of local electromagnetic fields to the modulation of the optical response.[5, 26-36] The ability of tuning the optical response by applying an external electric potential has been also demonstrated,[37, 38] as well as the improvement in the nonlinear optical behaviour.[39, 40] In particular, the photocurrent generation in hybrid graphene/plasmonic systems attracted a great deal of interest for the realization of photodetectors with tunable response in the visible to mid infrared and, in perspective, to obtain photovoltaic devices with improved efficiency.[13-15, 41] Besides, the combination of plasmonic light scattering and optimal electric conductivity of the nanohybrids has been applied to enhance the photocurrent generation in organic photovoltaic cells.[42, 43] Composite materials containing noble metal NPs and graphene derivatives have been investigated also for their visible-light photocatalytic response, positively tested against the destruction of pollutant or toxic molecules.[26, 44-47]

On the other hand, the cooperative effect of plasmonic and graphene absorption has been exploited to obtain superior light-to-heat conversion efficiency, with various purposes such as photothermal therapy of cancer, photoacoustic imaging or antimicrobial action.[48-52]

Multiple sensing applications are based on the surface plasmon resonance of noble metals coupled with graphene-based materials, showing remarkable results in the detection of DNA,[53]

biomolecules,[54] and even gases.[55] One of the reasons contributing to the superior performances of hybrid SPR sensors is due to the action of graphene sheets as spacers between metal NPs, which limits plasmon broadening by interparticle plasmon coupling.[56]

A large number of investigations concerned the amplification of the surface enhanced Raman scattering (SERS) effect in noble metal – graphene hybrids.[57-63] This has been applied for the ultrasensitive detection of various analytes,[5, 8, 59] as well as to obtain detailed information on graphene itself[57, 61, 64, 65] or on the local field enhancement of the plasmonic substrate.[58, 66] Interestingly, the chemical-physical stability of graphene and its derivatives found application in the stabilization of the plasmonic substrates for SERS.[67-70] This is especially desired in case of silver nanoparticles which easily undergo to oxidation and etching in air or in liquid environment.[68-70]

In hybrid plasmonic-graphene nanostructures, a crucial role is played by the SPR response after coupling of the metal NPs with the graphene moiety. In fact, it is well known that SPR is highly sensitive to composition, size, shape, dielectric environment and interface chemistry of the metal NPs, in a way which can induce either amplification or damping of the plasmon response, with direct consequences on the optical performances of the nanodevice.[1-3, 71, 72] On the other hand, modelling plasmonic properties of such nanohybrids can provide useful indications for the synthesis, for instance allowing *in situ* monitoring of products in a fast and easy way by UV–visible spectroscopy.

Here we used the discrete dipole approximation (DDA) method[72-74] to study the SPR of silver and gold NPs in proximity of graphene flakes or embedded in graphene structures. SPR modifications in metal NPs with different shape, such as spheres, rods and disks, have been compared. Besides, the effect of the morphology of NPs-graphene nanohybrids was investigated in a step-by-step approach which goes from NPs facing a graphene flake to NPs embedded in a graphene matrix. Our calculations show that SPR is sensibly influenced by the presence of graphene, although Ag and Au NPs may have opposite behaviours for specific combinations of particle size, shape and assembly. Our results help in the characterization of this class of nanostructures, and in guiding the synthesis of plasmonic NPs / graphene nanohybrids with different levels of structural complexity and optimized photonic properties.

Methods.

Optical properties of nanohybrids were evaluated by the DDA method.[72-74] The DDA is able to calculate the extinction of electromagnetic waves by objects with arbitrary geometries and complex refractive index.[73, 75, 76] In the DDA it is assumed that the object is interacting with a monochromatic plane wave incident from infinity.[73, 75, 76] The main advantage of the DDA is that it

is completely flexible regarding the geometry of the object, because the structure of interest, called "target", is replaced by N polarizable points (i.e. N cubic dipoles) arranged in a cubic lattice with same geometry and permittivity of the original object.[73-76] Calculations of the extinction cross section are accurate provided that the target adimensional "size parameter" $2\pi a_{eff} / \lambda < 25$,[73, 75, 76] where λ is the wavelength of the incident photons and a_{eff} is connected to target volume V by

$$V = \frac{4}{3} \pi a_{eff}^3 \qquad (1).$$

DDA theory was first proposed by Purcell & Pennypacker, and then reviewed and developed by Draine, Goodman and Flatau.[73, 75, 76] The basis of the DDA is that the polarization P_j induced on each dipole j of position r_j and polarizability p_j is given by

$$\overline{P_j} = p_j \overline{E}_{Loc}\left(\overline{r}_j\right) \qquad (2)$$

where E_{Loc} is the electric field originated by the incident radiation of amplitude E_0, and includes the contribution of all other dipoles:

$$\overline{E}_{Loc}\left(\overline{r}_j\right) = \overline{E}_0 \, exp\left(i\overline{k} \cdot \overline{r}_j + i\omega t\right) - \sum_{l \neq j} \overline{\overline{A}}_{jl} \overline{P}_l \qquad (3)$$

where $\overline{\overline{A}}_{jl}$ is the interaction matrix and $\overline{E}_{inc}\left(\overline{r}_j\right) = \overline{E}_0 \, exp\left(i\overline{k} \cdot \overline{r}_j + i\omega t\right)$ is the incident monocromatic plane wave with frequency ω and wavevector $\overline{k}$.[73, 75, 76]

The full expression of $\overline{\overline{A}}_{jl} \overline{P}_l$ (in c.g.s. units) is:

$$\overline{\overline{A}}_{jl} \overline{P}_l = \frac{exp\left(ikr_{jl}\right)}{r_{jl}^3} \left\{ k^2 \overline{r}_{jl} \times \left(\overline{r}_{jl} \times \overline{P}_l\right) + \frac{\left(1 - ikr_{ij}\right)}{r_{jl}^2} \left[r_{jl}^2 \overline{P}_l - 3\overline{r}_{jl}\left(\overline{r}_{jl} \cdot \overline{P}_l\right)\right] \right\} \qquad (4)$$

where $\overline{r}_{jl} = \overline{r}_j - \overline{r}_l$, $r_{jl} = \left|r_j - r_l\right|$.

The extinction cross section (σ_{ext}) of the target is then given by

$$\sigma_{ext} = \frac{4\pi k}{\left|\overline{E}_0\right|^2} \sum_{j=1}^{N} \left(\overline{E}_{inc}^* \cdot \overline{P}_j\right) \qquad (5)$$

where $\overline{E}_{inc}^*$ is the complex conjugate of the incident electric field.[73, 75, 76]

A crucial point of the DDA is the use of an appropriate expression for p_j. In this work, calculations were performed with the DDSCAT software,[75] where p_j is expressed according to the lattice dispersion relation (LDR) developed by Draine and Goodman,[73-75] i.e. as a correction of the Clausius - Mossotti polarizability by a series expansion of $k \cdot d$ and ε_m, with d the interdipole spacing and ε_m the matrix dielectric constant:

$$p_j^{LDR} = \frac{p_j^{CM}}{1 + p_j^{CM}\left[b_1 + b_2\varepsilon_j + b_3 S\varepsilon_j\right]\left(\dfrac{k^2}{d}\right)} \qquad (6)$$

where ε_j is the dipole permittivity, b_1, b_2, b_3 and S are coefficients of the expansions, and p_j^{CM} is the Clausius-Mossotti polarizability

$$p_j^{CM} = \left(\frac{d}{3}\right)^3 \frac{\varepsilon_j - 1}{\varepsilon_j + 2} \qquad (7).$$

The expression for p_j developed by Draine and Goodman is valid only for interdipole spacing $d \ll \lambda$.[73, 75, 76] In this work, interdipole spacing was set to 0.335 nm, which in the majority of cases corresponded to the maximum number of dipoles N allowed by the software, and is related to the maximum computer memory available on scientific workstations.[75] In all cases N resulted between $5 \cdot 10^4$ and 10^6, as required to minimize computational errors on the absolute value of the extinction cross section and to allow reliable comparison between calculated optical properties.[71, 73-75, 77, 78]

Although the DDSCAT software supports calculations for a variety of target geometries (e.g., ellipsoids, cylinders, etc.), in the present case we deal with heterogeneous objects composed of metal and graphene, and therefore we exploited the ability of DDSCAT to import arbitrary target geometries into the code.[71, 74, 75, 79] The targets were generated ad hoc as a cubic array of point dipoles, each with well defined polarizability properties assigned according to whether they belong to the metal or to the graphene nanostructures, and disposed according to the geometry of the object under consideration.[71, 74, 79]

A remarkable advantage of the DDA is that target optical constants are introduced directly from experimental data into the calculation as input numerical parameters, independently of composition or geometry, and without any need for the interpolation with analytical models of the optical constants.[71, 74, 75] Therefore, optical constant of bulk silver and gold,[80] and the anisotropic optical constant of graphene[81] were adopted (see Figure S1 in S.I.). Besides, the optical constants of Ag and Au NPs were corrected for the intrinsic size effects according to what described by Kreibig,[71, 74, 82, 83] The intrinsic size effect is due to the conduction electrons mean free path being comparable to particles size l along the direction of polarization promoted by the electromagnetic field.[71, 74, 82, 83] In the reasonable assumption that only the free electron behaviour is affected by the size l of nanoparticles, the metal optical constant can be expressed in the following way:[71, 74, 82, 83]

$$\varepsilon(\omega, l) = \varepsilon_\infty(\omega) + \left[\omega_p^2\left(\frac{1}{\omega^2 + \Gamma_\infty^2} - \frac{1}{\omega^2 + \Gamma^2(l)}\right)\right] + i\left[\frac{\omega_p^2}{\omega}\left(\frac{\Gamma(l)}{\omega^2 + \Gamma_\infty^2} - \frac{\Gamma_\infty}{\omega^2 + \Gamma_\infty^2}\right)\right] \qquad (8)$$

where $\varepsilon_\infty(\omega)$ is the bulk value of the optical constant at frequency ω, Γ_∞ is the electrons relaxation frequency of the bulk metal, and $\Gamma(l)$ is the l-dependent value given by the following "size equation":

$$\Gamma(l) = \Gamma_\infty + A\frac{v_F}{l} \qquad (9)$$

with v_F the Fermi speed and A an empirical parameter usually set equal to 1 (for the full list of parameters see Table S1 in S.I.).[71, 82, 83]

The refractive index of the matrix surrounding the nanohybrid was set to $n_m = 1.334$. The value of n_m is typical of liquid environments such as water and is close to the "effective" refractive index of nanostructures located at the interface between air and solid substrates such as glass or polymers. At the same time, the value of n_m is not far from the refractive index of non absorbing inorganic and organic solid matrixes.

Results and Discussion.

Nanohybrids with Ag NSs. In a first approach to investigate the effect of graphene on the SPR of metal NPs, we considered the "ideal" case of a silver nanosphere (NS), with diameter $d = 10$ nm, located at variable distance (gap) from a circular graphene flake, with diameter of 50 nm, all embedded in a dielectric non-absorbing matrix (Figure 1a). The extinction cross section (σ_{ext}) of the nanohybrid was evaluated for a gap between the Ag NP and the gaphene flake varied in the 0.335 – 5 nm range. We considered electromagnetic radiation linearly polarized in parallel (Figure 1b) or transversal (Figure 1c) direction to the axis of the NPs – graphene hybrid.

Due to the highly anisotropic optical properties of graphene, coupling of the electric field with the electric dipole transition moments is not possible in parallel incidence (PI, Figure 1b), and the resultant absorption is very low (black dashed line in Figure 1b).[81] Hence, the extinction is dominated by the Ag NS, which shows the typical SPR band in proximity of 390 nm (red dashed line in Figure 1b).[71] We observe that the σ_{ext} of the nanohybrid does not change for gap between 5 and 0.335 nm, and it remains nearly identical to the extinction in case of inifinite gap between the two components, i.e. that obtained by the sum of σ_{ext} for isolated NP and flake (Figure 1b and S2a in S.I.).

Obviously, the optical absorption of graphene is much different when considering transversal incidence of electric field with hybrid axis (TI, Figure 1c and S2b in S.I.). TI allows the excitation of the van Hove singularity and of the continuum of electronic transitions peculiar of the two-dimensional graphene band structure, which generate respectively the band at ~275 nm and the flat absorption background in the whole spectral range (black dashed line in Figure 1c).[81] The SPR of

the isolated Ag NS is the same for PI and TI, and we observe from Figure 1c that there is no appreciable overlap between the characteristic peaks of the two nanomaterials. When considering the nanohybrid with TI, however, we have that SPR intensity descreases while decreasing the gap from 5 to 0.335 nm, and band width increases slightly. To obtain quantitative information on SPR evolution as a function of the gap between the Ag NP and the graphene flake, we extracted two parameters from the spectra in Figure 1c:

i) the change in SPR position for a given gap (SPR_{gap}), compared to that of the hybrid with inifinite gap (SPR_{∞}), expressed as

$$\Delta SPR = SPR_{gap} - SPR_{\infty} \qquad (10);$$

ii) the percent variation of σ_{ext} at SPR maximum for a given gap ($\sigma_{SPR(gap)}$), compared to that of the hybrid with infinite gap ($\sigma_{SPR(\infty)}$), expressed as

$$\Delta\sigma_{SPR} = 100 \cdot \frac{\left[\left(\sigma_{SPR(gap)} - \sigma_{graphene}\right) - \left(\sigma_{SPR(\infty)} - \sigma'_{graphene}\right)\right]}{\left[\sigma_{SPR(\infty)} - \sigma'_{graphene}\right]} \qquad (11)$$

where $\sigma_{graphene}$ and $\sigma'_{graphene}$ are the contribution of the graphene flake to extinction of the hybrid at the same wavelength of the SPR maximum. As shown in Figure 1d, when the gap reaches its minimum at 0.335 nm, ΔSPR and $\Delta\sigma_{SPR}$ have their maximum at, respectively, 2.7 nm and –13%, while they are nearly 0 already for a 5 nm gap.

We also investigated the effect of NPs size in the TI configuration (the only one with appreciable changes of σ_{ext}) by considering Ag NSs with d = 5 and 15 nm (Figures 1e and 1f, respectively, whose magnification is shown in Figures S2c and d). In all cases, SPR intensity decreases with the gap, although the effect is of lower entity for d = 15 nm than for the d = 5 and 10 nm (see the $\Delta\sigma_{SPR}$ plot in Figure 1d). Red shift of SPR is observed in all cases and with comparable entity (see the ΔSPR plot in Figure 1d).

On the one hand, red shift and moderate broadening of SPR is usually associated with the increase of the dielectric constant of the surrounding medium, which is what happens to the NPs while reducing the gap in the nanohybrid. On the other hand, quenching of the SPR is due to the fact that graphene absorption is non-zero in the UV-visible range.
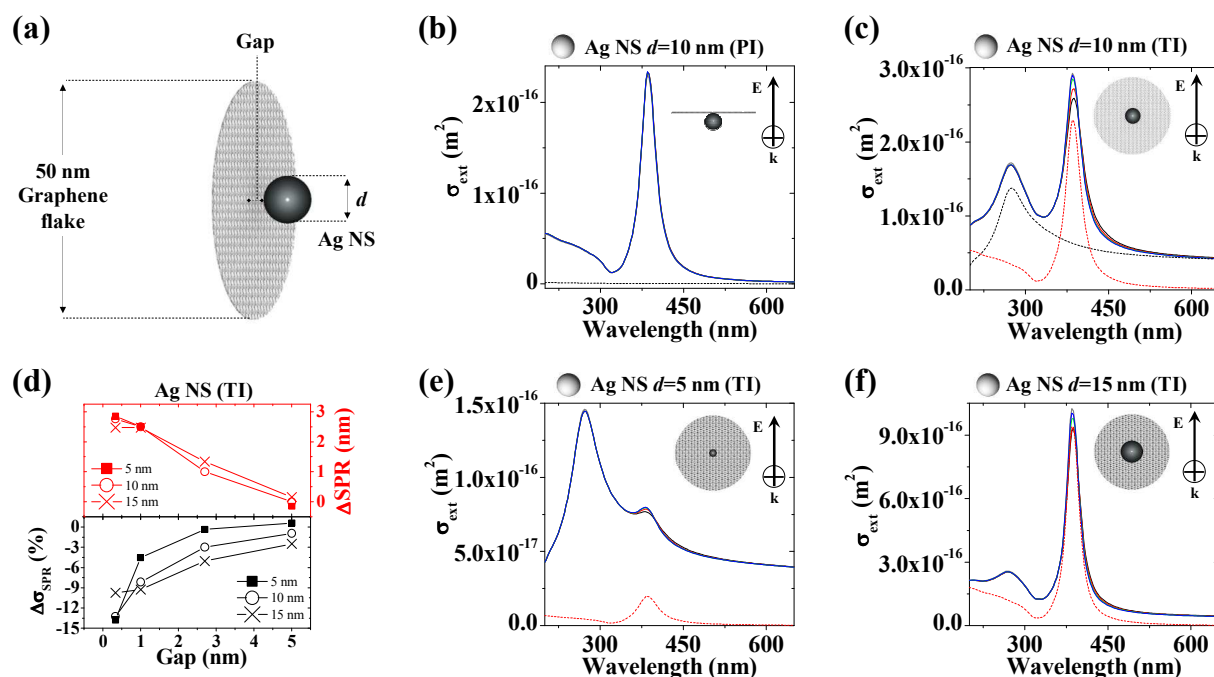
Figure 1. (a) Nanohybrid composed of an Ag NS, with diameter d, and a graphene flake, with diameter of 50 nm. The gap between the two objects is varied in the 0.335 – 5 nm range. **(b)** σ_{ext} of the nanohybrid for Ag NPs with size d = 10 nm, calculated for electric field polarized parallel to the NPs - flake axis (PI) at different gap values (black: 0.335 nm, red: 1 nm, green: 2.7 nm, blue: 5 nm). In all cases, the σ_{ext} are overlapped and no difference is appreciable. The σ_{ext} of the isolated 10 nm Ag NP (dashed red line) and of the graphene flake (dashed black line) are also shown for sake of comparison, and the sum of these two σ_{ext}, corresponding to the σ_{ext} of a nanohybrid with infinite distance between graphene and the Ag NS, is reported in grey. **(c)** Same as in (b) but considering the electric field with transversal incidence (TI) to the NPs - flake axis. In this case, the decrease of the SPR band is observed by decreasing the gap. **(d)** Changes in SPR position (ΔSPR, red symbols) and relative intensity ($\Delta\sigma_{SPR}$, black symbols), computed with reference to the hybrid with infinite gap, for Ag NPs with d = 5 nm (squares), 10 nm (circles) and 15 nm (crosses). As a reference we considered the nanohybrid with infinite gap. **(e)** Same as in (c) but considering a d = 5 nm Ag NS. **(f)** Same as in (c) but considering a d = 15 nm Ag NS. The magnification of the SPR region of Figures 1b, c, e, f is shown in Figure S2 in S.I..

Nanohybrids with Au NSs. The effect of NPs composition was investigated by considering a gold NS in the same nanohybrid geometry considered for the Ag NS, as shown in Figure 2a. The optical extinction of Au NSs is characterized by an SPR band in proximity of 520 nm, partially overimposed with the tail of interband transitions at shorter wavelengths (red dashed line in Figure 2b-c).[71, 82, 83] In case of PI, we observed the same trend of Ag, namely negligible effects on the SPR while decreasing the gap (Figure 2b and S3a in S.I.). Conversely, in TI (Figure 2c and S3b in S.I.), the SPR of Au NPs increases slightly with gap reduction. In particular, the maximum of $\Delta\sigma_{SPR}$ is obtained for a gap of 0.335 nm and is of +1.5%, with a SPR red shift of less than 1 nm for the d =

10 nm Au NS (Figure 2d). For $d = 5$ nm, SPR intensity changes of +5% and a red shift of ~3 nm is observed with the smallest gap (Figure 2d-e and S3c in S.I.). For $d = 15$ nm, almost no SPR changes, in terms of both intensity and red shift, are observed (Figure 2d-2f and S3d in S.I.).

We interpreted the SPR increase in 5 nm and 10 nm Au NSs as the effect of resonance red shift when the particle approaches the graphene flake. In fact, the partial overlap of plasmon resonances with the tail of interband transitions in Au NSs lowers the plasmonic performances in comparison to Ag analogues. Following Blaber,[84] this can be easily quantified using the plasmonic quality factor Q_{SPR}, expressed as

$$Q_{SPR} = -\frac{\varepsilon'}{\varepsilon''} \qquad (11)$$

where ε' and ε'' are, respectively, the real and imaginary (lossy) part of the metal optical constant. Q_{SPR} of gold rapidly increases with photon wavelengths (see Figure S4 in S.I.), explaining for instance the occurrence of a sharper longitudinal SPR in Au nanorods (NRs) than in Au NSs.[71, 79, 82, 84] Therefore, when the Au NS approaches the graphene flake, the effective dielectric constant of NP's environment also increases, inducing the slight red shift of SPR toward a spectral region with a more favourable Q_{SPR}, ultimately producing also the small increase of plasmon band intensity. In Au NSs, this effect compensates and exceeds slightly the shielding of the SPR due to graphene absorption in the TI configuration. Besides, graphene absorption is 30% larger in proximity of 400 nm, where Ag NSs have their SPR, than at 520 nm, where the plasmon resonance of Au NSs is located.
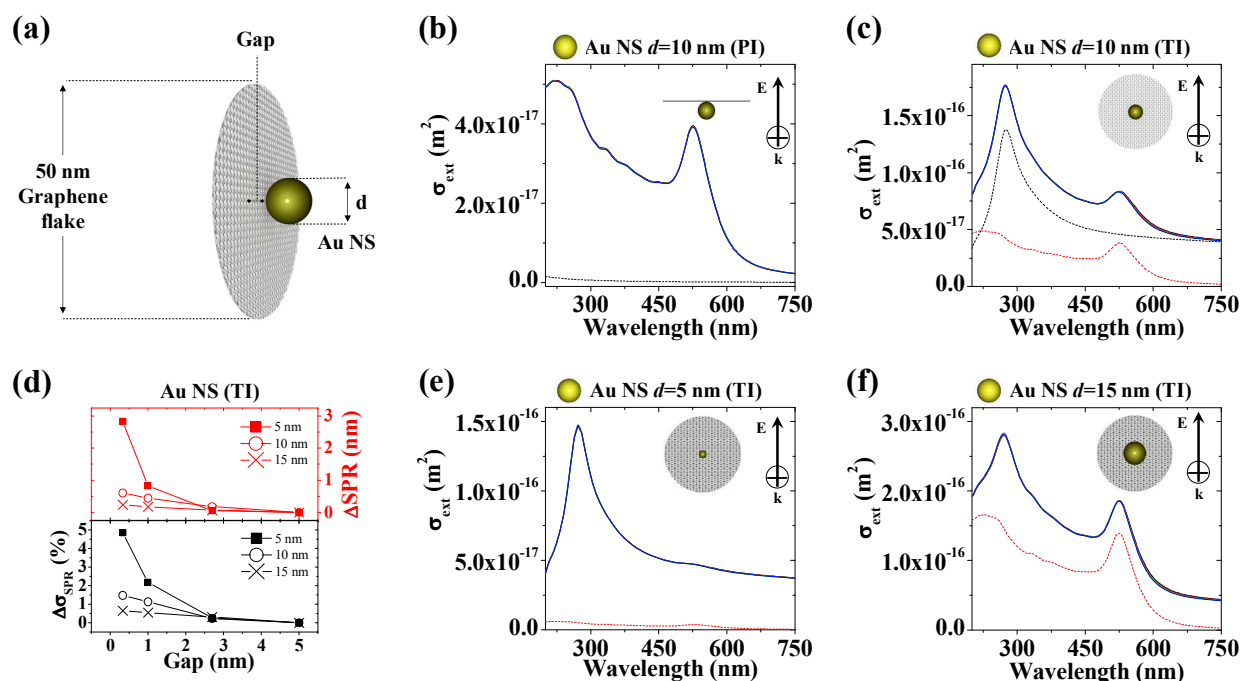
Figure 2. (a) Nanohybrid composed of an Au NS, with diameter d, and a graphene flake, with diameter of 50 nm. The gap between the two objects is varied in the 0.335 – 5 nm range. **(b)** σ_{ext} of the nanohybrid for a d = 10 nm Au NP, calculated for PI at different gap values (black: 0.335 nm, red: 1 nm, green: 2.7 nm, blue: 5 nm). In all cases, the σ_{ext} are overlapped and no difference is appreciable. The σ_{ext} of the isolated 10 nm Au NP (dashed red line) and of the graphene flake (dashed black line) are also shown for sake of comparison, and the sum of these two σ_{ext}, corresponding to the σ_{ext} of a nanohybrid with infinite distance between graphene and the Au NS, is reported in grey. **(c)** Same as in (b) but considering TI to the NPs - flake axis. **(d)** ΔSPR (red symbols) and $\Delta\sigma_{SPR}$ (black symbols) for Au NPs with d = 5 nm (squares), 10 nm (circles) and 15 nm (crosses). As a reference we considered the nanohybrid with infinite gap. **(e)** Same as in (c) but considering a d = 5 nm Au NS. **(f)** Same as in (c) but considering a d = 15 nm Au NS. The magnification of the SPR region of Figures 2b, c, e, f is shown in Figure S3 in S.I..

Nanohybrids with NRs and NDs. More insights about the changes of SPR in metal NPs – graphene hybrids can be obtained by studying nonspherical shapes such as nanorods (NRs) or nanodisks (NDs), which are frequently encountered in literature.[31, 37, 56, 61, 69, 85, 86] In case of NRs, we considered a spheroid with longitudinal axis of 25 nm and transversal axis of 10 nm (Figure 3a-b and S5a-b in S.I.), located at variable distance form a 50 nm graphene flake, i.e. with same configuration of the Ag and Au NSs described above. Optical properties of Ag and Au NRs in TI configuration are characterized by a sharp plasmon band in the red (dashed red lines in Figures 3a-b), due to the coherent excitation of electrons in longitudinal direction. In TI, we observed a remarkable decrease of longitudinal SPR intensity in both Ag and Au NRs when nanohybrid gap is reduced (Figure 3a-b). The changes in SPR intensity are quantified in –32% and –20% of $\Delta\sigma_{SPR}$ for, respectively, Ag and Au NRs at minimum distance from the flake (see $\Delta\sigma_{SPR}$ plot in Figure 3c).

10

Besides, SPR red shift up to +6 nm was calculated for both compositions (see ΔSPR plot in Figure 3c).

Quenching of the SPR by reducing the distance between metal NPs and graphene is confirmed also in case of Ag and Au NDs with diameter of 15 nm and height of 10 nm (Figure 3d-e and S5c-d in S.I.). Similar to NRs, the optical properties of Ag and Au NDs are dominated by a sharp plasmon band at wavelength longer than in NSs, which actually is the sum of the two degenerate electron excitations along the two plain faces of the disk. However, also other plasmon resonances with low intensity exists at shorter wavelengths in Ag, while in Au all bands are convoluted in a single peak due to the lower Q_{SPR} (i.e. to the larger bandwidth). In TI and at the minimum gap of 0.335 nm, the hybrids have $\Delta\sigma_{SPR}$ of −38% and −16% for Ag and Au respectively. The trend of SPR position versus gap is more complicated in NDs (see ΔSPR plot in Figure 3f) than in NRs and NSs, since the maximum of +2.5 nm for Ag and of +5.5 nm for Au is found for a gap of 1 nm, instead than at the minimum distance of 0.335 nm. Interestingly, for a gap of 0.335 nm, the ΔSPR of the Ag ND is −5.5 nm, and this blue shift is accompanied by a shrinking of the main SPR band (see black line in Figure 3d). Indeed, since the SPR in NDs is the convolution of multiple plasmon modes, the blue shift may be related to the different dielectric environment probed at the opposite faces of the disk when the gap is at its minimum value of 0.335 nm.

SPR modifications are more intense for NRs and NDs than for NSs, in fact spheroidal and discoidal particles have higher polarizability, i.e. higher sensitivity to the optical constant of the environment, than spherical particles with same composition.[72, 82, 87] This suggests that coupling of the SPR with the graphene flake is sensibly affected by the structural parameters and related polarizability of the metal NP.

Besides, the fact that SPR decreased in Au NRs and NDs by approaching the graphene flake, contrary to what happens with Au NSs, is in agreement with the above observation that the plasmon resonance is partially damped by overlap with the tail of interband transitions in spherical gold NPs. In Au NRs and NDs, the main SPR is located at longer wavelengths, where the lossy part of the optical constant is lower and the Q_{SPR} is higher, i.e. a condition in which the same trend for Au and Ag NPs is expected and observed.
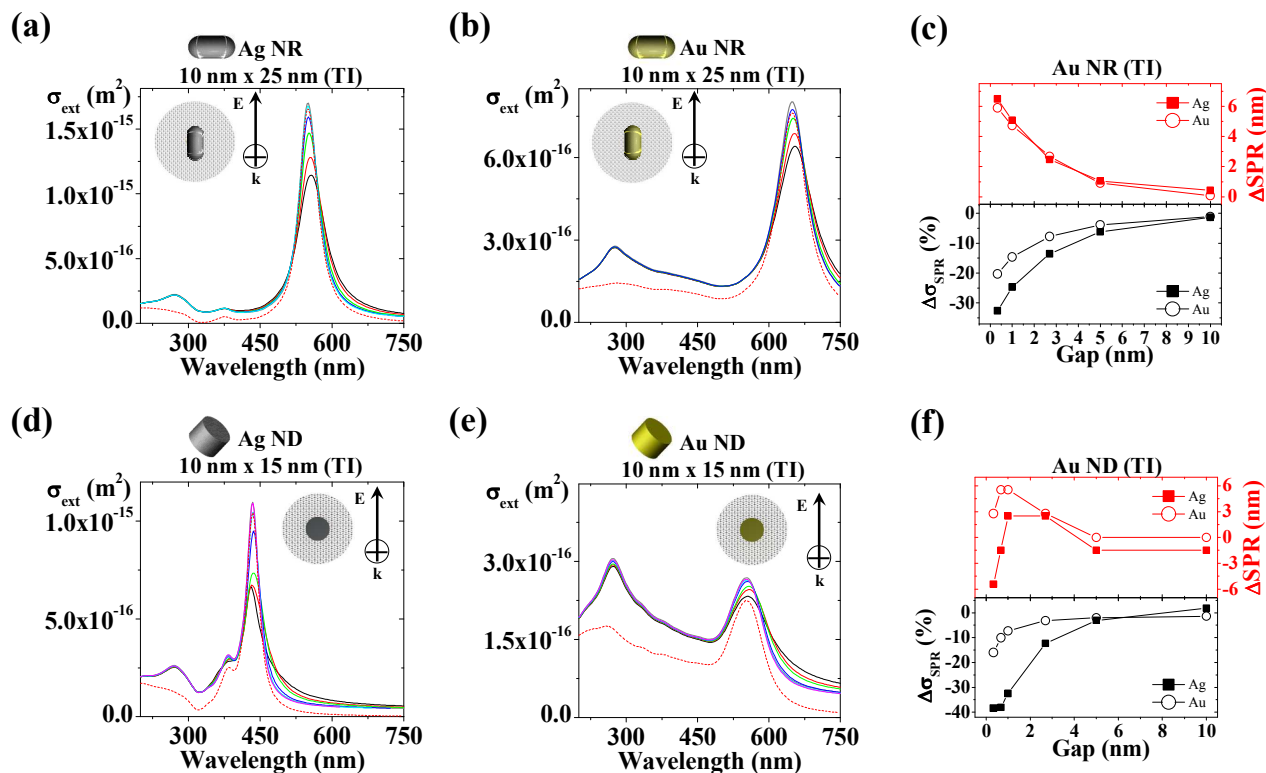
Figure 3. (a) σ_{ext} calculated for TI in case of a nanohybrid made of a spheroidal Ag NR, with short axis of 10 nm and long axis of 25 nm, and a graphene flake, with diameter of 50 nm. The gap between the two objects is varied in the 0.335 – 5 nm range (black: 0.335 nm, red: 1 nm, green: 2.7 nm, blue: 5 nm). The reference σ_{ext} of the graphene flake and the Ag NR for infinite gap is in grey. **(b)** Same as in (a) but for an Au NR. **(c)** ΔSPR (red symbols) and $\Delta\sigma_{SPR}$ (black symbols) for Ag (full squares) and Au (hollow circles) NRs. As a reference we considered the nanohybrid with infinite gap. **(d)** Same as in (a) but for an Ag ND with diameter of 15 nm and height of 10 nm. **(e)** Same as in (d) but for an Au ND. **(f)** ΔSPR (red symbols) and $\Delta\sigma_{SPR}$ (black symbols) for Ag (full squares) and Au (hollow circles) NDs. The magnification of the SPR region of Figures 3a, b, d, e is shown in Figure S5 in S.I..

Nanohybrids with holed graphene flakes. Graphene flake can exert a twofold influence on the SPR of nearby metal nanoparticles, due to shielding of NPs, or to alteration of their dielectric surrounding. To obtain more information about the role of these two effects, we considered hybrid nanostructures in which the graphene flake has an empty region (hole) with the same profile of the NPs (see Figure 4). In this way, shielding of NPs is reduced because of the lack of physical overlap with graphene along the direction of propagation of the electromagnetic wave, while the effect on the dielectric surrounding is still appreciable. In these calculations, we maintained at 0.335 nm the gap between the graphene flake and the NPs, which is the value with maximum effects.

When comparing the optical properties of NSs and NRs in proximity of the holed flake (red lines in Figures 4a-b) with the non-holed flake case (black lines in Figures 4a-b for 0.335 nm gap), we

observed much lower SPR modification. In fact, the SPR in hybrids with holed flakes is similar to that of the hybrid with infinite gap and non-holed flake (grey lines in Figures 4a-b).

Ag and Au NDs deserves a separate discussion because disc edges have relevant weight on the plasmonic response of these particles, and the edge is closer to the graphitic structure than in rounded particles such as NSs and NRs. This explains why SPR in hybrids with NDs and holed flake (red lines in Figure 4c) is more similar to the nonholed hybrid with gap of 0.335 nm (black lines in Figure 4c) than with infinite gap (grey lines in Figure 4c).

A different behaviour is observed in the case of NPs embedded in the middle of the same holed graphene flake (blue lines in Figure 4). In this configuration, changes to SPR are enhanced in comparison with the reference case of hybrids with nonholed flake and 0.335 nm gap, namely the SPR intensity is lower in Ag NS, Ag NR and Au NR, and higher in Au NS. Again, the NDs require a separate discussion, because the two plane faces are at 5 nm from the flake when the disk (whose height of 10 nm) is embedded in the middle of the hole. At this distance, the graphene flake has low influence on the edges and faces of the disc, hence optical properties (blue lines in Figure 4c) are similar to the case of the hybrid with nonholed flake and infinite gap (grey line in Figure 4c). In practice, the NDs have opposite behaviour than NSs and NRs, at parity of hybrid structure, due to different localization of plasmon oscillation.

These differences can be appreciated in a more quantitative way in Figure 5, where we reported the *ΔSPR* (red symbols) and $\Delta\sigma_{SPR}$ (black symbols) for the three cases of NPs at 0.335 nm from the holed flake (Figure 4a), at 0.335 nm from the non holed flake (Figure 4b) and embedded in the middle of the holed flake (Figure 4c).

Overall, this set of calculations confirmed that overlap between the flake and the NPs is not the main factor affecting SPR modification, whereas the change in dielectric properties in proximity of NPs is the dominating factor. In particular, the maximum effect is observed when the dielectric changes occur close to the portion of NPs surface where the plasmon resonance is localized. The fact that graphene has nonzero imaginary part of the optical constant in the whole visible range accounts for the decrease of SPR intensity, with the exception of Au NSs and Au NDs. Besides, the real part of graphene optical constant accounts for the red shift and, in case of Au NSs and Au NDs, also for the consequent modest increase of the SPR.

It is worth to emphasize how calculations showed that the total σ_{ext} in the range of the plasmon excitation of Ag NPs and Au NRs sensibly decreased due to the presence of graphene. Since the graphene itself is a not transparent material, this result is not trivial, because it means that the association with another non-transparent material (i.e. the plasmonic NPs) produces an overall decrease in optical density in the SPR spectral range.
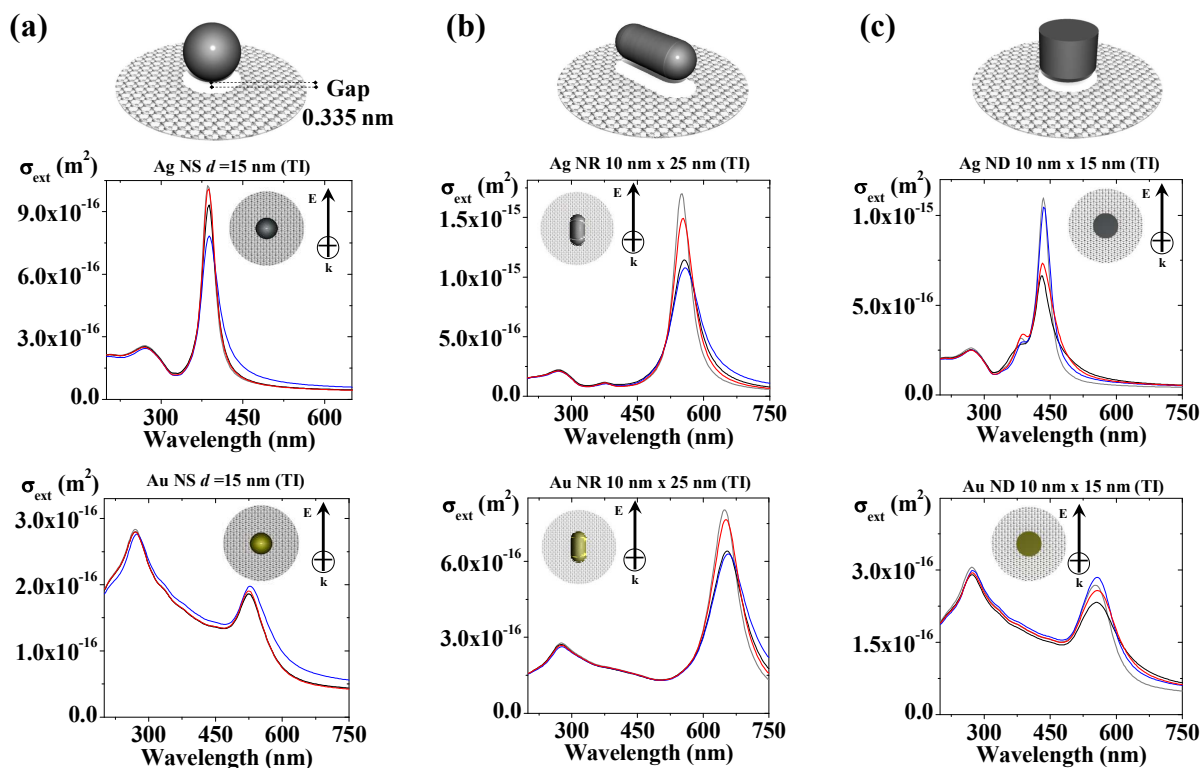
Figure 4. (a) σ_{ext} calculated for TI in case of a nanohybrid made of a spherical Ag (top) or Au (bottom) NP, with $d = 15$ nm, and graphene flake, with diameter of 50 nm and hole with the same profile of the NP (see sketch in the Figure). The gap between the two objects is set at 0.335 nm (red lines). Also the case for NPs embedded in the middle of the graphene flake is reported (blue lines). The reference σ_{ext} of the graphene flake and the Ag NR for infinite gap (grey lines), and the hybrid with gap of 0.335 nm in case of non-holed graphene flake (black lines) are also reported. **(b)** Same as in (a) but for an Ag (top) and Au (bottom) NRs with length of 25 nm and width of 10 nm. **(c)** Same as in (a) but for an Ag (top) and Au (bottom) NDs with diameter of 15 nm and height of 10 nm.
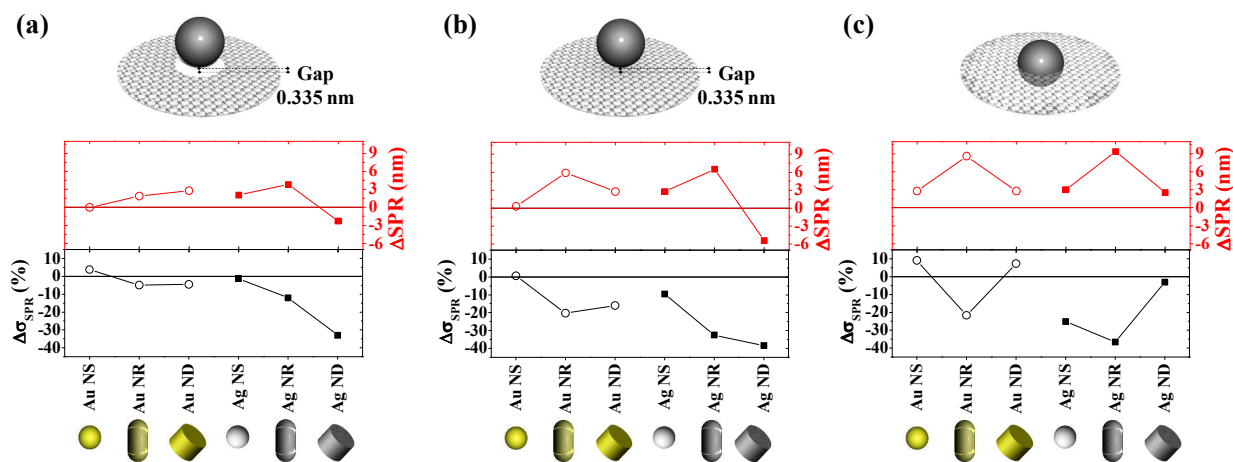

Figure 5. Plot of ΔSPR (red symbols) and $\Delta\sigma_{SPR}$ (black symbols) in Ag (black squares) and Au (hollow circles) NPs of nanohybrids described in Figure 4 for **(a)** holed graphene flake and gap of 0.335 nm, **(b)** non-holed graphene flake with gap of 0.335 nm, and **(c)** NPs embedded in the middle of the holed graphene flake.

Sandwich of NS between graphene. Since the coupling of the plasmon resonance with the graphene flake is sensibly affected by structural parameters of the metal NPs, one would expect that the SPR undergoes a larger modification when the NP is placed between two graphene flakes, in a sandwich configuration (Figure 6a). In our calculations, we considered d = 10 nm NSs and flake-NPs gap of 0.335 nm on each side. As expected, the SPR of Ag NS is further quenched in the sandwich configuration (red line in Figure 6b), whereas no modifications are observed for the Au NS (red line in Figure 6c). In particular, $\Delta\sigma_{SPR}$ of Ag NS passed from −13% with one flake to −20% with two flakes (black symbols in Figure 6d), with a change in ΔSPR from +2.8 nm to +5.0 nm. In the Au NS, a ΔSPR of +1 nm is observed, but without any increase of SPR intensity, probably because the advantage of such a limited red shift is completely compensated by the shielding of the additional flake. Interestingly, these calculations showed that SPR changes do not depend linearly on the number of flakes, and that the first graphene layer has the maximum effect on the plasmon properties of the metal NPs. The fact that SPR position in the sandwich is not significantly modified compared to the single flake hybrid is attributed to the fact that, in TI, the dipolar plasmon mode is predominantly localized at the equator of the NS, which is the part of the NP at maximum distance from the two flakes.[82]

Besides, we observe a slight decrease of the van Hove singularity at 275 nm in the sandwich. Since this is not observed in the hybrid with just one graphene layer, it is not due to the metal NS but it should be interpreted as graphene "self-shielding". Therefore, graphene shielding of optical extinctions is a general phenomenon not limited to the SPR.
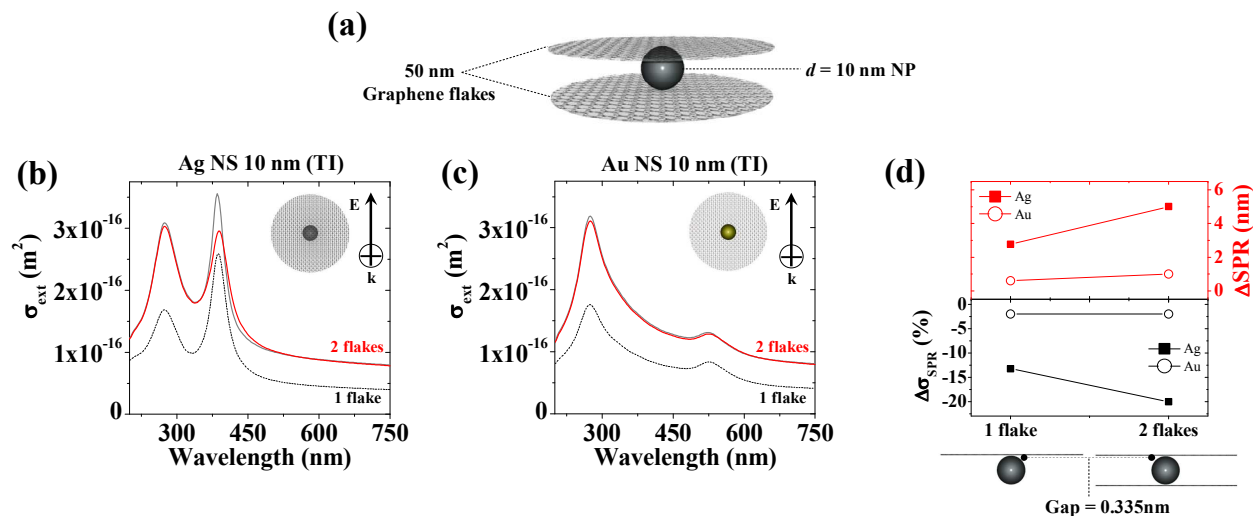

Figure 6. Nanohybrid made of a metal NS, with d = 10 nm, sandwiched between two graphene flakes with diameter of 50 nm **(a)**. The gap between the NS and flakes is 0.335 nm on each side. **(b)** σ_{ext} calculated for TI in case of Ag NS. The reference σ_{ext} of the graphene flake and the Ag NR for infinite gap is in grey. **(c)** Same as in (b) but for an Au NS. **(d)** ΔSPR (red symbols) and $\Delta\sigma_{SPR}$ (black symbols) for Ag (full squares) and Au (hollow circles) NPs.

NS embedded in graphene. The effect of wrapping metal NPs in graphene was investigated further by considering a nanosphere (d = 10 nm) embedded in the flake for a fraction (a/d) of its diameter variable between 0.13 and 0.93 (Figure 7 and S6 in S.I.). Several experimental studies showed that wrapping occurs when the graphene flake is overimposed to metal NPs, for the behaviour similar to a veil of this 2D material.[30, 37, 57, 58, 62] According to calculations, wrapping has the effect of amplifying the changes of SPR already observed in the nanohybrids of Figures 1 – 2. In fact, SPR of the Ag NS is quenched and red shifted, while SPR of the Au NS is red shifted and moderately augmented in intensity. From the quantitative point of view, $\Delta\sigma_{SPR}$ of Ag NS is –27% already for a/d = 0.13, reaching values as high as –40% for a/d > 0.5. With Au NS, SPR enhancements of +10-13% are achieved for a/d > 0.5. The red shift increases in both cases up to a ΔSPR of +13 nm and +9 nm for, respectively, Ag and Au NS.
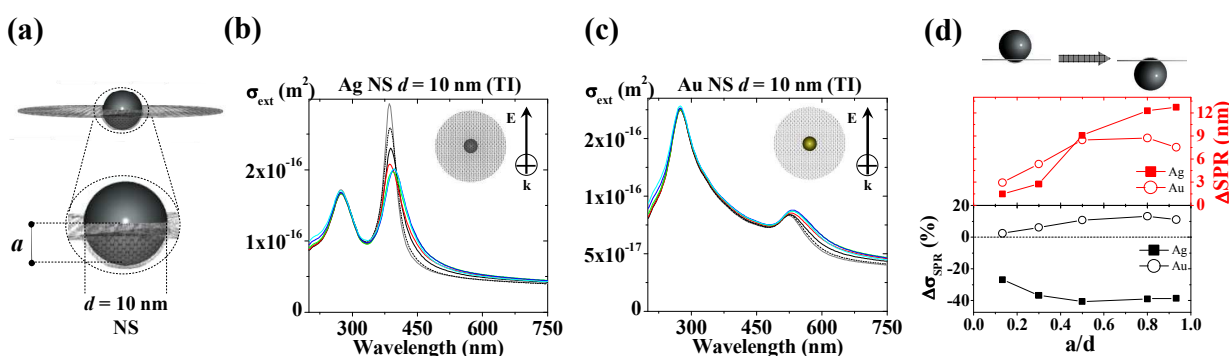

Figure 7. Nanohybrid made of a metal NS, with d = 10 nm, embedded in a 50 nm graphene flake for a fraction a/d of its diameter varied between 0.13 and 0.93 **(a)**. **(b)** σ_{ext} calculated for TI in case of Ag NS (black: a/d = 0.13, red: a/d = 0.30, green: a/d = 0.50, blue: a/d = 0.80, cyan: a/d = 0.93). The reference σ_{ext} of the graphene flake and the Ag NR for infinite gap is in grey, and the nanohybrid with 0.335 nm gap is the black dashed line. **(c)** Same as in (b) but for an Au NS. **(d)** ΔSPR (red symbols) and $\Delta\sigma_{SPR}$ (black symbols) for Ag (full squares) and Au (hollow circles) NPs. The magnification of the SPR region of Figures 7b, c is shown in Figure S6 in S.I..

Core@shell and nanocage hybrids. When the NS is completely embedded in a graphene flake, it can be described as a core@shell with a metal core and a graphitic shell. Therefore, the optical properties of core@shell nanohybrids have been investigated for Ag and Au NPs, also as a function of the number (n) of graphene layers enveloping the core (Figure 8a). These structures are often encountered in literature,[67, 68, 88] finding application as sensors or SERS substrates with improved stability. Calculations show that, just with 1 graphene shell, the SPR of the Ag NS is remarkably quenched compared to the isolated Ag particle (Figure 8b), with a $\Delta\sigma_{SPR}$ of –39% and a ΔSPR of +8 nm (Figure 8d). For increasing n, the quenching and red shift dramatically increase up $\Delta\sigma_{SPR}$ = –

85% and ΔSPR = +88 nm at n = 10. The nanohybrid with Au NS shows a similar dependence on n (Figure 8c), with $\Delta\sigma_{SPR}$ = –3% and ΔSPR = +3 nm at n = 1, progressively increasing up to $\Delta\sigma_{SPR}$ = –53% and ΔSPR = +72 nm at n = 10. This marks a difference with the SPR increase observed for the Au nanohybrid of Figure 7c-d, and it is attributed to the superior shielding ability of the complete graphene shell (Figure 7a) compared to the partial envelope of the NS (Figure 8a). Indeed, already in case of the embedded Au NS, the plot of $\Delta\sigma_{SPR}$ in Figure 7d showed a maximum increment at a/d = 0.8, with a trend reversal at a/d = 0.93.

The case of metal NS embedded in a cubic cage composed by a miltilayer of graphene was also considered (Figure 8e). The thickness of the graphene layer was varied between n = 1 and 10, where n = 1 means that the minimum thickness of the box is equivalent to a single graphene flake on each side (see Figure 8e), and so on for larger n. As expected, SPR quenching and red shift is larger in this type of nanohybrid, since the fraction of graphitic material is larger compared to the core@shell. Even for a minimum thickness of the box equivalent to a single graphene flake on each side of the box (n = 1), the $\Delta\sigma_{SPR}$ of the Ag NP is –77% and ΔSPR is +55 nm. For n = 10, $\Delta\sigma_{SPR}$ reaches –86% and ΔSPR increases up to +111 nm. Again, Au NP show the same trend, with $\Delta\sigma_{SPR}$ and ΔSPR of, respectively, -15% and +41 nm at n = 1, and of -35% and +97 nm at n = 10.

Overall, the trend in optical properties of core@shells and nanocages, as shown in Figures 8, is in agreement with experimental results reported in literature for nanocomposite of metal NPs and graphene.[19, 20, 22, 23, 25, 28, 30] The remarkable result of these calculations is that the overall absorption in the SPR region is sensibly diminished by coupling metal NS with the graphene multilayers. This result is not trivial considering that graphene layers are not transparent, but contributes to the overal absorption cross section of the nanohybrid. Therefore, coupling plasmonic NPs with graphene multilayers is an efficient way to dramatically change the optical density in the SPR region without acting directly or irreversibly on the metal nanostructure.
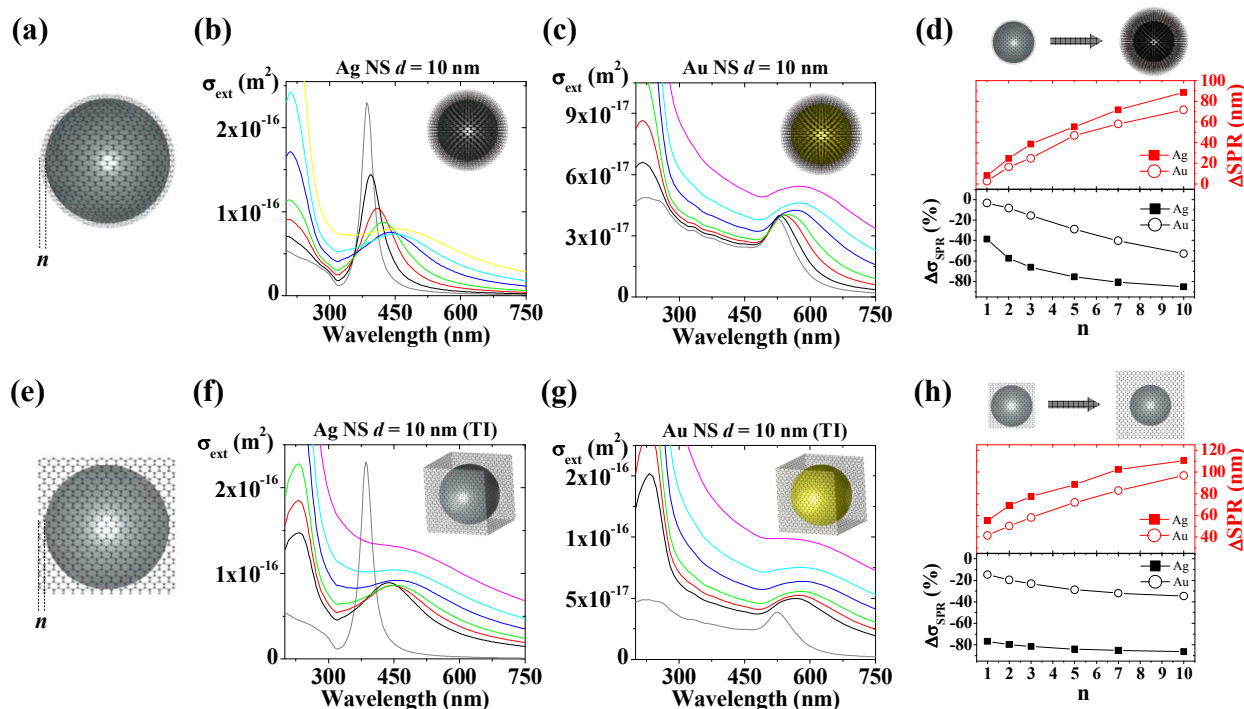
Figure 8. (a) Core@shell nanohybrid composed by a metal NS core ($d = 10$ nm) and a shell of n graphene layers. **(b)** σ_{ext} calculated in case of Ag NS with $n = 1$ (black), 2 (red), 3 (green), 5 (blue), 7 (cyan) and 10 (violet). The reference σ_{ext} of the isolated NS is in grey. **(c)** Same as in (b) but for an Au NS. **(d)** ΔSPR (red symbols) and $\Delta\sigma_{SPR}$ (black symbols) for Ag (full squares) and Au (hollow circles) NSs. **(e)** Nanocage nanohybrid composed by a metal NS core ($d = 10$ nm) embedded in a cubic multilayer graphene cage. **(f)** σ_{ext} calculated in case of Ag NS with minimum thickness equal to a number of graphene layers n of 1 (black), 2 (red), 3 (green), 5 (blue), 7 (cyan) and 10 (violet). The reference σ_{ext} of the isolated NS is in grey. **(g)** Same as in (b) but for an Au NS. **(h)** ΔSPR (red symbols) and $\Delta\sigma_{SPR}$ (black symbols) for Ag (full squares) and Au (hollow circles) NSs.

Conclusions.

In summary, we performed a systematic study on the SPR of metal NPs in proximity of a graphene flake or embedded in graphene structures, using the DDA method. The effect of NPs size and shape, the distance from graphene and the morphology of the graphene flake (entire, holed, wrapped, shell or multilayers) where investigated in a step-by-step approach. Results showed that SPR of Ag NPs is quenched and red shifted in nanohybrids. The same trend in generally observed with Au NPs, although specific configurations with limited wrapping allow a moderate SPR enhancement. The effect of graphene on the SPR becomes negligible already for a distance of the order of 5 nm, whereas it is relevant below 1 nm. The trend of the optical properties obtained by these numerical calculations are in agreement with several experimental results reported in literature for metal NPs / graphene hybrid materials.

Since the nanohybrids generally have lower absorption in the SPR spectral region, it is interesting to note that plasmon absorption is weakened by graphene, that is another light-absorbing material. In other words, calculations showed that coupling plasmonic NPs with graphene multilayers is an efficient way to dramatically change the optical density in the SPR region, without acting directly or irreversibly on the metal nanostructure. Since the integration of Ag and Au NPs with graphene is frequently sought for the realization of hybrid materials with optical, photoelectric and photocatalytic applications, these results are useful to guide the characterization and monitoring the synthesis of similar nanostructures, as well as for the development of nanohybrids with desired optical properties. Besides, these results can suggest new ways to assemble metal nanoparticles and graphene to obtain smart plasmonic nanohybrids with reversible optical properties.

Supporting Information.

The following supporting information is available: optical constants of Ag, Au and graphene; table of the parameters for the free electrons in Ag and Au; magnification of the SPR region of Figures 1, 2, 3 and 7; plot of Q for Ag and Au.

Bibliography.

1) M. Rycenga, C. M. Cobley, J. Zeng, W. Li, C. H. Moran, Q. Zhang, D. Qin and Y. Xia, *Chem. Rev.,* 2011, **111**, 3669.

2) P. K. Jain, X. Huang, I. H. El-Sayed and M. A. El-Sayed, *Plasmonics,* 2007, **2**, 107-118.

3) S. Eustis and M. A. El-Sayed, *Chem. Soc. Rev.,* 2006, **35**, 209-217.

4) E. Ringe, B. Sharma, A. Henry, L. D. Marks and R. P. Van Duyne, *Phys. Chem. Chem. Phys.,* 2013, **15**, 4110-4129.

5) A. C. Ferrari, F. Bonaccorso, V. Fal'Ko, K. S. Novoselov, S. Roche, P. Bøggild, S. Borini, F. H. Koppens, V. Palermo and N. Pugno, *Nanoscale,* 2015, **7**, 4598-4810.

6) A. K. Geim and K. S. Novoselov, *Nat. Mater.,* 2007, **6**, 183-191.

7) F. Bonaccorso, Z. Sun, T. Hasan and A. C. Ferrari, *Nat. Photon.,* 2010, **4**, 611-622.

8) P. Innocenzi, L. Malfatti and D. Carboni, *Nanoscale,* 2015, **7**, 12759-12772.

9) Y. Francescato, V. Giannini, J. Yang, M. Huang and S. A. Maier, *ACS Phot.,* 2014, **1**, 437-443.

10) Garcia de Abajo, F Javier, *ACS Phot.,* 2014, **1**, 135-152.

11) X. Huang, X. Qi, F. Boey and H. Zhang, *Chem. Soc. Rev.,* 2012, **41**, 666-686.

12) G. R. S. Iyer, J. Wang, G. Wells, S. Guruvenket, S. Payne, M. Bradley and F. Borondics, *ACS nano,* 2014, **8**, 6353-6362.

13) T. J. Echtermeyer, P. Nene, M. Trushin, R. V. Gorbachev, A. L. Eiden, S. Milana, Z. Sun, J. Schliemann, E. Lidorikis and K. S. Novoselov, *Nano Lett.,* 2014, **14**, 3733-3742.

14) Y. Yao, R. Shankar, P. Rauter, Y. Song, J. Kong, M. Loncar and F. Capasso, *Nano Lett.,* 2014, **14**, 3749-3754.

15) Z. Fang, Y. Wang, Z. Liu, A. Schlather, P. M. Ajayan, F. H. Koppens, P. Nordlander and N. J. Halas, *Acs Nano,* 2012, **6**, 10222-10228.

16) P. Kanade, P. Yadav, M. Kumar and B. Tripathi, *Plasmonics,* 2015, **10**, 157-164.

17) Z. Osváth, A. Deák, K. Kertész, G. Molnár, G. Vértesy, D. Zámbó, C. Hwang and L. P. Biró, *Nanoscale,* 2015, **7**, 5503-5509.

18) J. Mertens, A. L. Eiden, D. O. Sigle, F. Huang, A. Lombardo, Z. Sun, R. S. Sundaram, A. Colli, C. Tserkezis, J. Aizpurua, S. Milana, A. C. Ferrari and J. J. Baumberg, *Nano Lett.,* 2013, **13**, 5033-5038.

19) R. Muszynski, B. Seger and P. V. Kamat, *J. Phys. Chem. C,* 2008, **112**, 5263-5266.

20) J. Li and C. Liu, *Eur. J. Inorg. Chem.,* 2010, **2010**, 1244-1248.

21) K. Subrahmanyam, A. K. Manna, S. K. Pati and C. Rao, *Chem. Phys. Lett.,* 2010, **497**, 70-75.

22) Z. Xu, H. Gao and H. Guoxin, *Carbon,* 2011, **49**, 4731-4738.

23) F. He, J. Fan, F. Song, L. Zhang and H. L. Chan, *Nanoscale,* 2011, **3**, 1182-1188.

24) S. Z. Nergiz, N. Gandra and S. Singamaneni, *Carbon,* 2014, **66**, 585-591.

25) N. T. Lan, N. X. Dinh, N. D. Hung, H. Lan, P. A. Tuan, N. N. Trung, N. Q. Hoa, T. Q. Huy, N. Van Quy and T. Duong, *J. All. Comp.,* 2014, **615**, 843-848.

26) M. Zhu, P. Chen and M. Liu, *ACS nano,* 2011, **5**, 4529-4536.

27) Q. HuoáLiu, *Nanoscale,* 2013, **5**, 7785-7789.

28) J. Niu, Y. J. Shin, J. Son, Y. Lee, J. Ahn and H. Yang, *Opt. Expr.,* 2012, **20**, 19690-19696.

29) A. M. Zaniewski, M. Schriver, J. G. Lee, M. Crommie and A. Zettl, *Appl. Phys. Lett.,* 2013, **102**, 023108.

30) S. Zhang, X. Zhang, X. Liu, Z. Yin, H. Wang, H. Gao and Y. Zhao, *Appl. Phys. Lett.,* 2014, **104**, 121109.

31) A. Hoggard, L. Wang, L. Ma, Y. Fang, G. You, J. Olson, Z. Liu, W. Chang, P. M. Ajayan and S. Link, *ACS nano,* 2013, **7**, 11209-11217.

32) V. Kravets, F. Schedin, R. Jalil, L. Britnell, K. Novoselov and A. Grigorenko, *J. Phys. Chem. C,* 2012, **116**, 3882-3887.

33) E. Thouti, V. Kumar, P. K. Parashar, G. Reddy, R. Pasricha and V. K. Komarala, *Plasmonics,* 2015, , 1-7.

34) J. Wu, W. Shi and N. Chopra, *Carbon,* 2014, **68**, 708-717.

35) K. Zhang, H. Zhang and C. Li, *Phys. Chem. Chem. Phys.,* 2015, **17**, 12051-12055.

36) W. Wang, D. He, J. Duan, M. Fu, X. Zhang, H. Wu, Y. Hu and Y. Wang, *Phys.Chem.Chem.Phys.,* 2014, **16**, 4504-4509.

37) J. Kim, H. Son, D. J. Cho, B. Geng, W. Regan, S. Shi, K. Kim, A. Zettl, Y. Shen and F. Wang, *Nano Lett.,* 2012, **12**, 5598-5602.

38) N. K. Emani, T. Chung, X. Ni, A. V. Kildishev, Y. P. Chen and A. Boltasseva, *Nano Lett.,* 2012, **12**, 5202-5206.

39) B. S. Kalanoor, P. B. Bisht, S. Akbar Ali, T. T. Baby and S. Ramaprabhu, *JOSA B,* 2012, **29**, 669-675.

40) A. R. Sadrolhosseini, A. Noor, N. Faraji, A. Kharazmi and M. A. Mahdi, *J. Nanomater.,* 2014, **2014**.

41) U. J. Kim, S. Yoo, Y. Park, M. Shin, J. Kim, H. Jeong, C. Baik, Y. Roh, J. Lee and K. Im, *ACS Phot.,* 2015, **2**, 506-514.

42) M. Chuang and F. Chen, *ACS Appl. Mater. Interf.,* 2015, **7**, 7397-7405.

43) G. Fan, Q. Zhuo, J. Zhu, Z. Xu, P. Cheng, Y. Li, X. Sun, S. Lee and J. Tang, *J. Mater. Chem,* 2012, **22**, 15614-15619.

44) S. K. Bhunia and N. R. Jana, *ACS Appl. Mater. Interf.,* 2014, **6**, 20085-20092.

45) Y. Li and N. Chopra, *Phys. Chem. Chem. Phys.,* 2015, **17**, 12881-12893.

46) R. Rajesh, E. Sujanthi, S. S. Kumar and R. Venkatesan, *Phys. Chem. Chem. Phys.,* 2015, **17**, 11329-11340.

47) X. Liang, T. You, D. Liu, X. Lang, E. Tan, J. Shi, P. Yin and L. Guo, *Phys. Chem. Chem. Phys.,* 2015, **17**, 10176-10181.

48) A. F. Zedan, S. Moussa, J. Terner, G. Atkinson and M. S. El-Shall, *ACS nano,* 2012, **7**, 627-636.

49) H. Moon, D. Kumar, H. Kim, C. Sim, J. Chang, J. Kim, H. Kim and D. Lim, *ACS nano,* 2015, **9**, 2711-2719.

50) D. Lim, A. Barhoumi, R. G. Wylie, G. Reznor, R. S. Langer and D. S. Kohane, *Nano Lett.,* 2013, **13**, 4075-4079.

51) D. Lin, T. Qin, Y. Wang, X. Sun and L. Chen, *ACS Appl. Mater. Interf.,* 2014, **6**, 1320-1329.

52) X. Shi, H. Gong, Y. Li, C. Wang, L. Cheng and Z. Liu, *Biomaterials,* 2013, **34**, 4786-4793.

53) O. Zagorodko, J. Spadavecchia, A. Y. Serrano, I. Larroulet, A. Pesquera, A. Zurutuza, R. Boukherroub and S. Szunerits, *Anal. Chem.,* 2014, **86**, 11211-11216.

54) S. Chen, X. Hai, X. Chen and J. Wang, *Anal. Chem.,* 2014, **86**, 6689-6694.

55) M. Cittadini, M. Bersani, F. Perrozzi, L. Ottaviano, W. Wlodarski and A. Martucci, *Carbon,* 2014, **69**, 452-459.

56) T. Maurer, R. Nicolas, G. Lévêque, P. Subramanian, J. Proust, J. Béal, S. Schuermans, J. Vilcot, Z. Herro and M. Kazan, *Plasmonics,* 2014, **9**, 507-512.

57) P. Wang, W. Zhang, O. Liang, M. Pantoja, J. Katzer, T. Schroeder and Y. Xie, *ACS nano,* 2012, **6**, 6244-6249.

58) S. Heeg, R. Fernandez-Garcia, A. Oikonomou, F. Schedin, R. Narula, S. A. Maier, A. Vijayaraghavan and S. Reich, *Nano Lett.,* 2012, **13**, 301-308.

59) X. Li, W. C. Choy, X. Ren, D. Zhang and H. Lu, *Adv. Funct. Mater.,* 2014, **24**, 3114-3122.

60) A. Mcleod, K. C. Vernon, A. E. Rider and K. Ostrikov, *Opt. Lett.,* 2014, **39**, 2334-2337.

61) F. Schedin, E. Lidorikis, A. Lombardo, V. G. Kravets, A. K. Geim, A. N. Grigorenko, K. S. Novoselov and A. C. Ferrari, *ACS nano,* 2010, **4**, 5617-5626.

62) W. Xu, J. Xiao, Y. Chen, Y. Chen, X. Ling and J. Zhang, *Adv. Mater.,* 2013, **25**, 928-933.

63) S. Sun and P. Wu, *Phys. Chem. Chem. Phys.,* 2011, **13**, 21116-21120.

64) W. Park, *J. Phys. Chem. C,* 2014, **118**, 6989-6993.

65) Y. Xiao, Y. Francescato, V. Giannini, M. Rahmani, T. R. Roschuk, A. M. Gilbertson, Y. Sonnefraud, C. Mattevi, M. Hong and L. F. Cohen, *Phys. Chem. Chem. Phys.,* 2013, **15**, 5395-5399.

66) Q. Hao, B. Wang, J. A. Bossard, B. Kiraly, Y. Zeng, I. Chiang, L. Jensen, D. H. Werner and T. J. Huang, *J. Phys. Chem. C,* 2012, **116**, 7249-7254.

67) Y. Liu, Y. Hu and J. Zhang, *J. Phys. Chem. C,* 2014, **118**, 8993-8998.

68) Z. Song, Z. Chen, X. Bian, L. Zhou, D. Ding, H. Liang, Y. Zou, S. Wang, L. Chen and C. Yang, *J. Am. Chem. Soc.,* 2014, **136**, 13558-13561.

69) J. C. Reed, H. Zhu, A. Y. Zhu, C. Li and E. Cubukcu, *Nano Lett.,* 2012, **12**, 4090-4094.

70) X. Li, J. Li, X. Zhou, Y. Ma, Z. Zheng, X. Duan and Y. Qu, *Carbon,* 2014, **66**, 713-719.

71) V. Amendola, O. M. Bakr and F. Stellacci, *Plasmonics,* 2010, **5**, 85-97.

72) K. L. Kelly, E. Coronado, L. L. Zhao and G. C. Schatz, *J. Phys. Chem. B,* 2003, **107**, 668-677.

73) B. T. Draine and P. J. Flatau, *J. Opt. Soc. Am. A,* 1994, **11**, 1491–1499.

74) A. L. Gonzalez, C. Noguez, G. P. Ortiz and G. Rodriguez-Gattorno, *J. Phys. Chem. B,* 2005, **109**, 17512-17517.

75) B. T. Draine and P. J. Flatau, *http://arxiv.org/abs/1002.1505,* 2010.

76) J. Goodman, B. T. Draine and P. J. Flatau, *Opt. Lett.,* 1991, **16**, 1198-1200.

77) A. Ishikawa, K. Osono, A. Nobuhiro, Y. Mizumoto, T. Torimoto and H. Ishihara, *Phys. Chem. Chem. Phys.,* 2013, **15**, 4214-4225.

78) X. Xu, J. Luo, M. Liu, Y. Wang, Z. Yi, X. Li, Y. Yi and Y. Tang, *Phys. Chem. Chem. Phys.,* 2015, **17**, 2641-2650.

79) V. Amendola, R. Sajia, O. M. Maragò and A. Iatì, *Nanoscale,* 2015, **19**, 8782-8792.

80) P. B. Johnson and R. W. Christy, *Phys. Rev. B,* 1972, **6**, 4370-4379.

81) V. Kravets, A. Grigorenko, R. Nair, P. Blake, S. Anissimova, K. Novoselov and A. Geim, *Phys. Rev. B,* 2010, **81**, 155413.

82) U. Kreibig and M. Vollmer, *Optical Properties of Metal Clusters*, Springer, Berlin, 1995.

83) V. Amendola and M. Meneghetti, *J. Phys. Chem. C,* 2009, **113**, 4277-4285.

84) M. D. Arnold and M. G. Blaber, *Opt. Expr.,* 2009, **17**, 3835-3847.

85) C. Xue, M. Gao, Y. Xue, L. Zhu, L. Dai, A. Urbas and Q. Li, *J. Phys. Chem. C,* 2014, **118**, 15332-15338.

86) H. Chen, C. Hsin, Y. Huang, M. L. Tang, S. Dhuey, S. Cabrini, W. Wu and S. R. Leone, *J. Phys. Chem. C,* 2013, **117**, 22211-22217.

87) C. F. Bohren and D. R. Huffman, *Absorption and scattering of light by small particles*, Wiley-Interscience, New York, 1983.

88) J. Wu, W. Shi and N. Chopra, *J. Phys. Chem. C,* 2012, **116**, 12861-12874.

TOC Text and Graph

Surface plasmon resonance (SPR) of Ag and Au nanoparticles (spheres, rods, discs) is damped when they are located at less than 5 nm from graphene flakes or embedded in graphene matrix.